Tracing back the origin of cell-cell communication: Hydra vulgaris releases extracellular vesicles delivering regulators of head and foot regeneration

Maria Moros
Instituto deNanociencia y Materiales de Aragón(INMA)
Eugenio Fergola
Istituto di Scienze Applicate e Sistemi Intelligenti “E. Caianiello”, Consiglio Nazionale delle Ricerche
Valentina Marchesano
CNR-ISASI
Margherita Mutarelli
Istituto di Scienze Applicate e Sistemi Intelligenti “E. Caianiello”, Consiglio Nazionale delle Ricerche
Giuseppina Tommasini
Istituto di scienze Applicate e Sistemi Intelligenti "E.Caianiello", Consiglio Nazionale delle Ricerche
Beata Miedziak
Istituto di scienze Applicate e Sistemi Intelligenti "E.Caianiello", Consiglio Nazionale delle Ricerche
Giuliana Palumbo
Istituto di Scienze Applicate e Sistemi Intelligenti “E. Caianiello”, Consiglio Nazionale delle Ricerche
Alfredo Ambrosone
Istituto di scienze applicate e sistemi intelligenti https://orcid.org/0000-0002-1897-4028
Angela Tino
Istituto di Scienze Applicate e Sistemi Intelligenti “E. Caianiello”, Consiglio Nazionale delle Ricerche
Claudia Tortiglione (claudia.tortiglione@cnr.it)
Istituto di scienze Applicate e Sistemi Intelligenti "E.Caianiello", Consiglio Nazionale delle Ricerche https://orcid.org/0000-0003-1447-7611

Article

Keywords: extracellular vesicles, hydra vulgaris, cell-cell communication

Posted Date: August 14th, 2021

DOI: https://doi.org/10.21203/rs.3.rs-763240/v1

Abstract

Recent body of evidence demonstrates that extracellular vesicles (EVs) represent the first language of cell-cell communication emerged during evolution. In aquatic environments, transferring signals between cells by EVs offer protection against degradation, allowing delivering of chemical information in high local concentrations to the target cells. The packaging of multiple signals, including those of hydrophobic nature, ensures target cells to receive the same EV-conveyed messages, and the coordination of a variety of physiological processes across cells of a single organisms, or at the population level, i.e. mediating the population´s response to changing environmental conditions. Here, we purified EVs from the medium of the freshwater invertebrate *Hydra vulgaris*, and the molecular profiling by proteomic and transcriptomic analyses revealed multiple markers of the exosome EV subtype. Moreover, positive and negative regulators of the Wnt/β-catenin signaling pathway, the major developmental pathway acting in body axial patterning, were identified. Functional analysis on amputated polyps revealed EV ability to interfere with both head and foot regeneration, suggesting an active role in setting up tissue gradients and oro-aboral polarity through delivery of short and long-distance signals. Our results open the path to unravel EV biogenesis and function in all cnidarian species, tracing back the origin of the cell-cell, cross-species or cross-kingdom communication in aquatic ecosystems

Introduction

Cell-cell communication is a mandatory condition for all the multicellular organisms as we know them; the possibility to exchange multiple and different signals between cells, at great distances or even between different organisms, supports the organism homeostasis and allows interacting with the surrounding environment. Intercellular cross-talk is achieved by various means, with the most straightforward one being the direct contact between communicating cells, also known as the juxtacrine signalling. Gap junctions are a well-known example of this form of communication and their functional characterization has been widely documented both in vertebrates and invertebrates [1, 2, 3]. Conversely, paracrine or endocrine signalling, namely the release and subsequent uptake of signalling factors, does not require a direct contact between donor and recipient cells, allowing for short- and long-distance intercellular communication. In addition to communication routes based on the secretion of soluble molecules in the extracellular space, the discovery of signalling factors embedded in bilayer lipid membrane structures, termed extracellular vesicles (EVs), has gradually expanded our view on how cellular cross-talk works. Despite the lack of general consensus about their classification and nomenclature [4] EVs are broadly divided into three main categories: apoptotic bodies, microvesicles and exosomes, mainly based on their different diameter and biogenesis route [5, 6].

First discovered in sheep reticulocyte cultures [7,8 9], exosomes are spheroidal nano-sized vesicles (30-150 nm) which originate during early-to-late endosome maturation. Multiple events of inward budding along the endosome membrane selectively gather proteins and nucleic acids from the cytosol into intraluminal vesicles (ILV). The late endosome is henceforth termed multivesicular body (MVB) and its fusion with the cell plasma membrane releases these vesicles into the extracellular space [10, 11, 12]. The protein content of exosomes partly reflects the biogenesis and maturation pathways that these vesicles undertake; consequently, specific proteins can be used as biochemical markers in order to confirm the presence of such vesicles in the isolated fractions. A fair number of tetraspanin transmembrane proteins, such as CD9, CD63 and CD81, are enriched in exosomes, reflecting the spatial reorganization that endosomal proteins go through before the formation of the MVB [13, 14]. Similarly, lysosomal-associated membrane proteins LAMP1 and LAMP2 are late endosomal markers and can usually be found in exosomes [11]. However, different populations of exosomes may have distinct molecular signatures [14, 15]. In fact, one fascinating feature of this type of EVs is that their content, comprising proteins, lipids and nucleic acids, is determined not only by the cell type they originate from, but also by the physiological state of the organism, resulting in major differences of these vesicles and their cargo in terms of quantity and quality [16]. Such diversity is in agreement with the many processes exosomes have been implicated into, such as parasitic host-pathogen interaction [17], viral infection, immune response, cardiovascular diseases, central nervous system disease, and cancer progression, shuttling

into the receiving cells nucleic acids, metabolites, lipid and proteins [12]. Of particular interest in cancer biology is their role in the 'education' of distant cells in order to create a pre-metastatic niche, thus promoting metastasis [18, 19, 20]. The intrinsic properties of exosomes in regulating complex intracellular pathways offer a new paradigm for their application as disease biomarkers, or as nanocarriers of therapeutic agents in cell-free therapies [21].

The wide portfolio of possible applications makes even more appealing the evolutionary study of EVs in model organisms, to increase our understanding in how they work and how they exert their functions in different contexts and environments. For instance, exosomes derived from *Drosophila melanogaster* have been identified as partly responsible for the establishment of Hedgehog (HH) and Wingless morphogenic gradients during the wing imaginal disc development [22, 23]. In *Caenorhabditis elegans* HH-related proteins are released on apical exosomes in a MVB-dependent manner involving V0-ATPase and P-4 ATPase activities [24,25]. However, very little is known about the role of EVs in aquatic environment. By virtue of their ability to transport abundant biological signals, to protect them from the highly heterogeneous and possibly damaging environment, and to increase the local concentration of one or more co-acting biomolecules that reach the target cells, EVs can have a profound impact on aquatic community structure and trophic level-interactions [26], providing important clues on interspecies and interkingdom relationships. Due to the conservation of key physiological mechanisms throughout the animal kingdom, evolutionary approaches to understanding EV biogenesis and bioactivity may profoundly impact on both fundamental and applied biology in vertebrates.

In this paper we report for the first time the presence of EVs in the freshwater cnidarian polyp *Hydra vulgaris* and characterized main morphological, biochemical and functional features. Classically used as a model organism in developmental biology, the structural simplicity of *Hydra* body offers many advantages for a variety of investigations, from environmental ecotoxicology to nanobiotechnology, allowing to study the impact of exogenous nanostructured compounds [27, 28, 29, 30] together with intracellular biotransformations and molecular responses [31, 32, 33] at animal, cell and molecular levels. The body wall is organized as a hollow tube, with an apical mouth opening surrounded by a ring of tentacles and a foot to anchor to a substrate. It is structured as a bilayer of epithelia, an ectoderm with epitheliomuscular cells facing the outer medium and an inner endoderm with all cells facing the body cavity, separated by an acellular mesoglea (Figure 1A-B). This tissue-like organization, with no organs and body fluids, is maintained by the continuous cell self-renewal and differentiation of three distinct stem cell lineages of endoderm, ectoderm, and interstitial stem cells, giving rise to a few differentiated cell type, i.e. neurons, gland cells, nematocytes and gametes [34, 35]. The plasticity and remodelling capacity of the body reaches the maximum expression during the regeneration process [34, 36, 37, 38]. Indeed, the ability to regrow the whole body from tissue pieces or even cell aggregates has made Hydra a one-of-a-kind platform to study regeneration processes and to shed some light on why some organisms have partially lost this ability [39]. The Wnt/b-catenin signalling pathway represents the major developmental pathway acting in adult *Hydra* to maintain the oro-aboral axis, and it is reactivated during injury and throughout the regeneration to rebuild missing structures from amputated polyps [40, 41, 42]. In addition, Wnt signalling is integrated by Notch-signalling, restricting the tentacle activation and re-establishing the head organizer during regeneration[43]. Functional and transcriptomic evidences have recently showed the early activation of the Wnt/b-catenin signalling pathway as part of a generic transcriptional response to injury, which initiates an oral patterning cascade independent from the tissue context[44, 45]. The outcome of this activation appears regulated by long range signals generated by tissue organizers located at both animal poles[44, 45, 46, 47, 48], whose existence was proposed 40 years ago, by means of classical tissue manipulation techniques [49, 50]. To date, no vehicles have been isolated for lipid-modified and poorly soluble signalling molecules. The EV function in developmental signalling, promoting the release and spread of canonical ligands and/or mediating the transfer of a variety of biologically active molecules from one cell to another is well documented[23, 51, 52]. This prompted us to search for similar EV mediated signalling mechanisms also in *Hydra*, and to shed light on novel cell-cell communication strategies acting in homeostatic and in regenerative contexts, at the beginning of animal evolution. We developed a strategy for EV purification from the polyp culture medium, characterized their morphology and their molecular content at protein and RNA levels, and showed their active role in modulation of both head and foot regeneration. The shuttling of functional molecules via EV in target cells shows that this mechanism of cell-cell

communication evolved early in animal evolution and may mediate not only physiological processes but also cross-species or cross-kingdom communication in aquatic ecosystems.

Results

Hydra vulgaris release round-shaped extracellular vesicles in the aquatic environment

Groups of 250 polyps collected into Petri dishes were starved for 4 days into 10 ml of Hydra medium. EVs were isolated from the medium by differential centrifugation, following a well-established protocol [53], slightly modified. Following removal of dead cells and cell debris the last centrifugations were performed at 70,000 x g rather than at 100,000 x g, as high speeds seem to promote the co-purification of contaminants such as protein complexes and aggregates [54]. Pelleted EVs were suspended in Phosphate buffered saline (PBS) and characterized by Transmission Electron Microscopy (TEM). Fig. 1C shows the round shape of isolated EV and the presence of double membrane around the electron dense vesicle (see also Fig. S1). By microfluidic resistive pulse sensing (MRPS) a yield of $5x10^{10}$ particles/mL was estimated from a typical preparation (250 polyps into 10 ml of medium), while the distribution of the particle size showed two peaks at 66 nm and 70.5 nm (Fig 1D and Fig. S1). A good correlation with these measurements was obtained through other approaches, such as Dynamic Light Scattering (DLS) analysis and TEM (Fig S1), both confirming the average size of 66 nm, and suggesting an enrichment in exosome-like vesicles. The presence of EVs on *Hydra* ectodermal cell surface was previously supposed during an ultrastructural study describing several inward and outward mechanisms negotiating the entrance, trafficking, and clearance of gold nanoparticles in animal tissues [55]. To confirm this evidence, *Hydra* polyps were pulsed (24 h) with positively charged AuNPs, synthesised as previously described [55] and 48 h later processed for TEM (Fig. S2). Semi-thin slices showed the presence of round nanovesicles decorated with AuNPs on the external membrane of ectodermal cells, laying into the glycocalix (Fig. 1E-F), confirming *in vivo* assembly of AuNP-EV structures as part of the secretory route [55]. The ability of EV to bound positively charged AuNP also *in vitro* was shown by incubating freshly isolated EVs with AuNPs, producing the same rosette-like nanostructures observed *in vivo* (Fig. S2). This self-assembly demonstrates the strong interaction between EV membranes and positively charged AuNPs, likely due to electrostatic interaction.

The ability of EVs to be internalized into *Hydra* tissues was investigated by labelling freshly isolated EVs with PKH67 and incubating living polyps up to 5 h. Distinct green fluorescent signals were found on the body column and tentacles 2 h post incubation and in single cells obtained by maceration of treated polyps, indicating an efficient uptake of EV into *Hydra* cells (Fig 1 G-I; Fig. S3). These signals became diffuse after 5 h, suggesting the internalization and processing of the EV into the recipient cells

Hydra EVs shuttle typical exosome-associated proteins and key components of axial patterning

In order to characterize the molecular content of the EV, immunoblot analyses were initially performed to identify biochemical markers of EV subclasses, i.e. exosome specific proteins such as the tetraspanin CD63 [14]. By comparing immunoblot of protein extracts from whole animal lysates and EVs, a greater expression of the CD63 protein was found in EV extracts compared to lysates, while similar amount of proteins cross-reacted with antibody against the highly abundant membrane protein annexin B12. Actin expression was found greatly enhanced in whole lysates compared to EVs (Fig. 2). Overall these results demonstrate the presence of some exosome-specific proteins on EV, and prompted us to perform a mass spectroscopy analysis for a more detailed protein characterization. Initially, a MALDI-TOF/TOF analysis performed on EV protein bands excised from an SDS-PAGE gel confirmed the identification of annexin B12, along with actin (Fig. S4). Then a large scale EV isolation was achieved from 8000 *Hydra*, and protein extracts were used for LC-ESI-MS/MS analysis and protein identification. The analysis from two biological replicates identified 52 proteins with a Mascot score >32 (Table S1). Table 1 shows selected unique *Hydra* proteins grouped for function. Remarkably, 29 proteins were present also into the Exocarta protein database (http://www.exocarta.org/), suggesting the exosome –like nature of the isolated EVs. The

exosome-specific proteins include two annexins, a synthenin1-like protein involved in the biogenesis of exosomes, a programmed cell death 6-interacting protein involved in the MVB formation and the CD151 antigen belonging to the Tetraspanin family. Among others, chaperones (heat shock proteins), cytoskeletal proteins (actin, Rab and tubulin), extracellular matrix and glycocalyx constituents (fibrillin 1; Mucin 5AC), and important components of cell-cell adhesion (protocadherin fat 4) or signalling pathways (NOD2, Nav2.1, Notch) were found. Interestingly, two uncharacterized proteins containing thrombospondin type-1 domain were found, whose role as a feedback inhibitor of Wnt signalling during *Hydra* body axis patterning and maintenance has been recently identified [56]. Altogether the variety of putative proteins identified in the Hydra EVs, either structural or involved in cell-cell communication and signal transduction, suggests multiple functional roles played by EVs in adult *Hydra*, and their correlation with known exosome proteomes.

Accession No.	Protein Name	Putative Function	Matched Peaks	Matched Peptide	Mascot Score	ExoCarta
Cytoskeletal Proteins						
CDG70628	Actin, cytoplasmic 1	Actin network	18	16	235	Yes
XP_002161913	Tubulin beta chain	Microtubule network	10	8	169	Yes
XP_004208788	Tubulin alpha-1D chain	Microtubule network	5	4	41	Yes
Extracellular Matrix Constituents						
XP_012558692	Fibrillin-1	Microfibril assembly	11	10	130	Yes
XP_002166874	Fibrillin-2 isoform X1	Microfibril assembly	9	7	125	Yes
XP_002159997	Mucin-5AC, partial	Glycocalyx constituent	5	4	86	Yes
XP_002154154	Latent-transforming growth factor beta-binding protein 4-like	Extracellular matrix constituent	12	12	80	Yes
Membrane Proteins						
NP_001296699	Annexin B12	Calcium-dependent membrane binding	7	4	100	No
XP_004212135	Protocadherin Fat 4, partial	Cell-cell adhesion	7	7	89	Yes
XP_004212674	Protocadherin Fat 1, partial	Cell-cell adhesion	17	17	71	Yes
XP_012553809	Annexin A4-like	Calcium-dependent membrane binding	14	13	61	Yes
XP_002165348	CD151 antigen	Exosome marker	5	5	56	Yes
XP_004211099	Usherin-like, partial	Laminin, N-terminal domain	2	2	47	No
Cell-Cell Communication and Signal Transduction						
XP_012559193	Neurogenic locus notch homolog protein 1, partial	Notch signalling	9	7	86	Yes
AAN87350	14-3-3 protein B	Ser/Thr phosphorylated proteins binding	2	2	54	No
XP_002156827	Ras-like GTP-binding protein RHO	Membrane and vesicle trafficking	2	2	52	Yes
XP_012560741	Uncharacterized protein LOC105846485	NOD-like receptor signaling pathway	7	6	32	--
AEW90237	Voltage-gated sodium channel Nav2.1, partial	Neuronal signaling in Hydra	15	15	34	No
XP_012554672	cAMP-dependent protein kinase type II regulatory subunit-like isoform X2	cAMP-mediated signaling pathway	5	4	42	Yes
XP_004209147	Cell division control protein 42 homolog	Small GTPase-mediated signal transduction	2	2	36	Yes
Others						

XP_002159321	Syntenin-1-like isoform X2	Biogenesis of exosomes	9	8	99	Yes
NP_001296663	Elongation factor EF1-alpha	Translation elongation factor	11	10	89	Yes
ABC25030	Heat shock protein 70	Stress-induced molecular chaperon	8	8	73	Yes
XP_002162060	Programmed cell death 6-interacting protein	Accessory protein of the ESCRT-III complex	10	9	43	Yes
XP_002155023	Polyubiquitin-B	Vesicle cargo sorting	11	7	43	Yes
XP_002156816	Uncharacterized protein LOC100207118	Thrombospondin type 1 domain	5	5	130	—
XP_012566106	Uncharacterized protein LOC100203042	Thrombospondin type 1 domain	3	2	42	—

Table 1. Name and putative function of selected proteins identified by ESI-MS/MS analysis.

A comprehensive transcriptomic analysis was performed on total RNA from purified EVs conducting pair-end next-generation sequencings. The sequenced reads were first aligned against the NCBI *Hydra vulgaris* reference genome (assembly Hydra_RP_1.0), where a percentage of 32% and 22% could be mapped. For gene expression quantification, the reads were also directly aligned using the program kallisto on the Hydra_RP_1.0 transcript sequences, where the total mapped reads on transcripts were 50% and 45% of the reads mapped on the genomic sequence. The presence of a subset of genes was confirmed in EV-derived RNA by using reverse transcription polymerase chain reaction PCR (RT-PCR). The selection was based on manual screening of genes already identified in EVs and exosomes (*hsp70* and *actin) or* belonging to the Wnt/b-catenin signalling pathway (*b-catenin*, and *Wnt3)*. We then used the minimum expression level in TPM of the validated genes to define an empirical detection threshold (0.4 TPM in at least one library). Using this definition, we selected 6100 detected genes, among which 5499 were protein-coding, 525 long non-coding and 31 tRNA genes. The detected genes were functionally annotated with the known associated Gene Ontology terms using OrthoDB to highlight the most important biological processes encoded by EV mRNA[57]. The full list of the GO categorized genes is provided in Supplementary file 1. Interestingly, this analysis revealed that the most abundant transcripts within the Molecular Functions GO category are related to catalytic activity (alcohol dehydrogenase, sulfite oxidase), proteases and proteinase inhibitors (cathepsin, several members of the astacin family, antistasin), hydrolase and transferase activity. Within the Cellular Component GO category the genes encoding for intracellular and cytoplasmic anatomical structures were highly abundant, such as actin, cophylin, α-tubulin chain, β tubulin chain, talin-2, secreted glycoproteins (mucin 2-like mucin 5AC-like), and LAMP, a well-known exosome marker. The transcripts categorized into the Biological processes GO class included the classes of protein metabolism (tRNA synthase, eIF3, eIF4, eEF1a, tRNAs), signal transduction pathways (G-protein coupled receptors, Rho family, guanidine nuclear exchange factors, Wnt3, gremlin) and response to stress (Hsp70, Hsp90, Superoxide dismutase, Glutamate dehydrogenase, thioredoxin-like).

Beside transcripts identification, lncRNA species were detected from the RNA-seq analysis. In one case the lncRNA was mapped adjacent to the mucin5AC gene locus, detected both at mRNA and protein levels, suggesting the possibility that EVs may shuttle all molecular components for immediate and late availability of key information in target cells. The association

of lncRNA with exosomes was first demonstrated by the analysis of human plasma-derived exosomes by RNA-seq [58], and has been recently functionally characterized and linked to disease, including a list of cancers, where they act via epigenetic regulation of key target genes. Their presence in *Hydra* EV might suggest a regulatory function in the receiving cells.

In order to map the EV cellular source in the animal body we used a recently-published single-cell RNA-seq (scRNA-seq) atlas[59] to match *Hydra* EV-associated genes with molecular signatures of specific cell clusters, which were grouped according to cell lineage (ectodermal, endodermal and interstitial cell lineage), or anatomical location (head, body column and foot) (Fig. 3).

An alignment rate of 12% was obtained and 4997 transcripts were detected, of which 2975 were found in at least one cell type in the scRNA annotated on Swiss-prot (TPM 0.2 in at least one library, Supplementary file 2). A large percentage of transcripts (48%) was clustered as specific of the interstitial cell lineage, while those derived from the ectodermal (12,7%) and endodermal cell lineage (9,45%) were less abundant. By subclustering the EV transcripts according to unique cell type expression, using the same cell categories and differentiation trajectories identified in the scRNA-seq [59], a remarkable contribute of basal disk cells, battery cells, neurons and nematoblasts emerged (Fig. 3B-C). A detailed analysis subclustering EV transcripts into cell types of each cell lineage is shown in Fig. S5. Overall this indicates the mixture of precise molecular information from multiple cell types in *Hydra* EVs. The list of the 5 top genes in each cell cluster is provided in Table S4 and the list of the 10 top genes identified matching the scRNAseq is shown in Table S5. Interestingly, many genes belonging to the Wnt/b catenin signalling pathway were identified (Table 2), including *Wnt3*, *b-catenin*, *naked cuticle* [45] together with some inhibitors such as *dkk1/2/4*[60, 61], *astacin*[62], *thrombospondin*[56], and *sp5*[63]. Remarkably, *dkk1/2/4* and *astacin* were found among the most abundant transcripts specific of zymogen and granular mucous gland cell classes, strongly indicating their role in restricting the head organizer activity in the hypostome. On the other side, *thrombospondin*, a recently characterized glycoprotein acting as feedback inhibitor of *Wnt* signaling during body axis patterning and maintenance[56], was present both at mRNA and protein levels, indicating a pivotal role played by EVs in the regulation of the head organizer formation. By comparing the EV transcriptome to the proteome the majority of annotated proteins (found also on exosome proteomes) was identified also at transcript level (*actin, tubulin, annexinB12, mucin 5AC, hsp70, astacin, thrombospondin, Notch …*) indicating the concomitant transfer of molecular information for immediate and programmed response in the target cells.

Genes involved in Wnt/β-catenin signaling pathway

Gene ID	Gene ID (NCBI)	Gene name	Wnt modulator	Lineage	Cell type	Anatomical region
t8678aep	100192274	Dickkopf 1/2/4-A	Negative regulator	Interstitial	i_zimogen gland cell	Body
t14102aep	100192275	dickkopf-like protein Dlp-1	Negative regulator	Interstitial	i_zimogen gland cell	Body
t1688aep	100192284	β-catenin	Positive regulator	Ectoderm, Interstitial	Ec_battery cell, i_neuron/gland_cell_progenitor	Tentacle, Body
t29291aep	101237470	transcription factor Sp5-like	Negative regulator	Ectoderm, Endoderm	Ec_battery cell, En_head, En_tentacle	Head
t11826aep	100199257	Tcf	Positive regulator	Endoderm, Interstitial	En_head, i_neuron_ec	Head, Body
t34763aep	100205238	naked cuticle	Negative regulator	Endoderm	En_head	Head
t13357aep	100199272	β-catenin-like protein 1	Positive regulator	Interstitial	i_female germline1, i_male germline, i_nb1, i_neuron/gland cell progenitor, i_SC, i_stem cell/progenitor	Body
t14194aep	100203050	Wnt3	Positive regulator	Endoderm	En_head	Head
t18735aep	100213948	FoxA/Budhead	Positive regulator	Interstitial	i_neuron/gland_cell_progenitor	Body
t31094aep	100215335	Foxd2-like		Endoderm	En_foot	Foot
t16296aep	100199630	HAS-7	Negative regulator	Interstitial	i_granular mucous gland cell, i_zymogen gland cell	Head, Body
t474aep	100214250	HmTSP	Negative regulator	Endoderm	En_tent-nem(pd), En_tentacle	Tentacle

Table 2 List of EV transcripts involved in the Wnt/β-catenin signalling pathway matching the scRNA-seq database

EVs modulate head and foot regeneration in *Hydra*

The finding in the EV transcriptome of both positive and negative regulators of the Wnt/b catenin pathway (Fig. 4A) prompted us to evaluate the EV bioactivity in receiving polyps. *Wnt3* gene transcript levels were shown upregulated in polyps treated with EV, both at 24 h and 48 h post treatment (Fig. 4B), suggesting for the first time the involvement of *Hydra* EV in the exogenous activation of Wnt signalling.

In addition to Wnt modulators, Notch was identified in the EV proteome and transcriptome, strongly supporting a role of EVs as contributing to the head organiser activity, carrying signals for local self-activation and long ranging inhibition. To verify this hypothesis, the role of Hydra EVs in the context of regeneration was tested. Freshly prepared EV were added to polyps amputated at midgastric level (50% of body column length), and the head regeneration efficiency was evaluated by morphometric analysis. Stumps of progressive developmental stage (stages 0, 1, 2 and 3) were monitored at regular intervals, starting at 24 h post amputation (p.a.) (Fig. 5A). At each time point significant differences were observed in the distribution of developmental stages, with the EV-treated stumps always presenting more advanced stages compared to the

controls (Fig. 5B). These results indicate a clear enhancement effect played by EV in the regeneration of the head. Similar results were also obtained when the amputation was sub-hypostomal (80% of upper body length) (Fig. S6), suggesting that EV cargo, when received by upper body cells behaves as an exogenous source of head activators. The impact of EVs on the ability of the lower body cells to regenerate a new foot was evaluated by bisecting whole polyps at 20% of the body length (Fig. 5C). The absence of distinctive morphological changes that characterize this process led us to use biochemical assays to monitor the differentiation of foot specific cells, based on the detection of peroxidase activity. This enzymatic activity is used as specific marker of basal disk cell differentiation, producing a strong signal at 36-48 h p.a[64]. While control regenerates showed a clear peroxidase-positive basal disk at 36 h p.a., there was only a faint staining in the basal disk region of EV treated foot regenerates at this time, indicating an inhibition of the foot regeneration process. Taken together, the molecular characterization of the EV cargo and the functional study suggest a regulatory role played by EV in *Hydra* for establishment and maintaining the oro-aboral axis during homeostasis and regeneration

Discussion

The production and release of EVs has been documented in all three domains of life, both in unicellular and multicellular organisms. Functional studies have demonstrated their involvement in a large number of processes, including morphogenesis and development, while increasing evidences suggest that they may also participate in intra- and inter-species communication [65, 66, 67]. The evolutionary conservation of this form of communication poses important questions about the role it might have had on the generation of complex life as we know it today [68 69]. Apart from our work detecting EV on *Hydra* ectodermal cell surface[55], so far no evidences documented their presence in Cnidarians, where they might act as signals for cell-cell communication, or as long range signals across species, or even kingdoms of aquatic life. We investigated their role in the transmission of molecular signals along the body and in the modulation of axial patterning during regeneration. In *Hydra* two stable tissue organizers located at the oral and aboral poles are responsible for the tissue polarity [46]. While the molecular bases of foot organizer are still largely unknown, the head organizer relies on the canonical Wnt/bcatenin pathway and other integrating signalling pathways, such as the Notch-Delta [70, 71, 72]. Using classical tissue manipulation techniques [49] and more recently gene transcript profiling [41, 44, 48] the presence of long-range inhibitory signals in *Hydra* head organizer has been supposed, acting in adults polyps to maintain the oral-aboral polarity and preventing the formation of ectopic organizers elsewhere in the body. Amputated organizers may transiently increase the ability of wounded tissue throughout the body column to form secondary axes, while during foot regeneration these inhibitory signals would prevent ectopic head formation at aboral-facing amputations [44] . To date, these signals have not been identified and in the present work we provide evidence that they could rely on EV released in the extracellular medium.

We purified and characterized EVs from *Hydra* culture medium by differential centrifugation, characterized their round-shaped and double-layered morphology via TEM and estimated the size in the range consistent with exosome EV subtype[73]. Proteomic analysis revealed numerous exosome markers, often related to their biogenesis route and cargo sorting mechanisms [74 15]. This evidence, together with the morphology, size and mRNA loading strongly suggests that the EV isolated are exosomes or are highly enriched in this vesicle subtype. Most of the identified proteins correlate with the transcripts, including proteinases, catalytic proteins and transcription factors, suggesting the delivery of key molecular information for early and late responses in the receiving cells. Moreover, a multitude of signalling components belonging to BMP, Notch and Wnt/bcatenin pathways among others were identified. The alignment of EV transcriptome with the scRNA-seq atlas recently produced[59] allowed to extract important information on the cell sources of EV transcripts. Under our condition of EV purification multiple cell types appeared involved in the loading and release of EVs. In addition to ectodermal cells expected to release EV, as facing the external medium, a large contribute to the EV transcriptome matched transcripts specific of the interstitial stem cell lineage, dispersed throughout the body column, especially neurons. This suggests that EVs may mediate the information flow within the *Hydra* non overlapping neural networks [75]. Finally, a minor fraction of transcripts was specific of endodermal cells, especially gland cells, which is consistent with their location, facing the gastric cavity, and their molecular repertoire of enzymatic activities and signalling factors, such as those restricting the Wnt signal in

the hypostome [56, 60, 62]. A comparative analysis between EVs produced by transgenic lines tagged in each cell lineage would help in the future to confirm this *in silico* evidence.

Concerning the possible role *in vivo*, the EV information tool-box may be used for cell-cell communication to maintain homeostatic condition, i.e. axis polarity, regulate animal size and tissue growth. In other conditions, i.e. during budding, regeneration or stress response, they may act to orchestrate coordinated cell responses between distant tissue regions, or among different polyps. In this work we purified EV from the medium of healthy polyps mirroring the condition used to enhance EV production from cell culture, i.e. starvation and crowding [76] and our omics and functional analyses are the outcomes of this particular state. EV may vary their molecular cargo under certain conditions, such as stress, reproduction, temperature changes, adapting the molecular information to deliver diverse messages to the cells, from hydrophobic signals to lipids, second messengers, or nucleic acids. We believe that by comparing the EV content produced under different physiological states different outputs might be produced, leading to decipher the “code” used by cells to communicate to distant cells or organisms about the environmental challenges.

We have demonstrated that treating amputated polyps with EVs, at a dosage far higher compared to the physiological condition, induces an enhancement of the head regeneration and a decrease in the foot regeneration efficiency. We explain these final outcomes as resulting from the release of key messengers acting as both positive and negative regulators of pivotal signalling pathways. Our focus on Wnt/bcatenin messengers identified several EV transcripts belonging to this pathway, especially Wnt inhibitors, leading to the hypothesis that the EV may represent the long distance signalling tools proposed since a long time ago for the determination of head and foot organizer tissue[44, 49]. In addition to mRNA, tRNA and lncRNA here detected, EV are known to vehicle micro RNA, small RNA, lipids, DNA and other metabolites[5], opening the path to further analyses for a deeper characterization of Hydra EV and unravel their role in cell-cell communication.

Methods

Animal culture

H. vulgaris (strain Zurich) was asexually cultured in *Hydra* medium (1 mM $CaCl_2$ and 0.1 mM $NaHCO_3$) at pH 7. The animals were kept at 18 ± 1°C and fed thrice a week with freshly hatched Artemia salina nauplii.

Hydra vulgaris handling and laboratory manipulation does not undergo ethical regulation

Collection of Extracellular Vesicles

For EV collection, 250 polyps were placed in 10 mL of Hydra solution in 6 cm Petri dishes. After 4 days starvation, Hydra conditioned medium was collected and centrifuged using a Beckman Coulter Avanti J-25 centrifuge (rotor JA-25.15) at 10,000*g* for 30 min to remove tissue patches and at 20,000*g* for 30 min to pellet any cellular debris. The resulting supernatant was then centrifuged at 74,200*g* for 150 min at 4 °C and the pelleted EVs were washed in Hydra solution, followed by one last centrifugation. Pelleted EVs were resuspended in either PBS or Hydra solution.

-

Transmission Electron Microscopy (TEM)

EVs were visualized using TEM following a slightly modified protocol to that reported by Thery et al [76]. Briefly, EVs were fixed with an equal volume of 4% paraformaldehyde and deposited onto a Formvar-carbon coated electron microscopy grid. Once dried, the grids were washed with PBS, fixed with 1% glutaraldehyde for 5 min and washed with distilled water 8 times. The

samples were stained with 1% ammonium molybdate for 2 min, dried and observed using a FEI Tecnai 12 120 kV or JEOL USA, Inc., USA) at 80kV Hydra polyps were dissected into appropriate pieces to fit into cup-shaped HPF specimen carriers. Tissue pieces were pipetted into a 0.2- or 0.3-mm deep carrier and covered with an additional carrier. Finally, the obtained sandwiches were cryo-immobilized by HPF. Frozen sandwiches were transferred into appropriate containers for storage in Liquid N2 for later use or subjected to freeze substitution (FS). The frozen samples were transferred under liquid N2 into cryo-vials containing frozen FS cocktails (anhydrous acetone plus 1% OsO4 and 0.1–0.2% uranyl acetate). Subsequently, the lids were screwed loosely onto the vials to permit safe evaporation of excess N2 gas. The vials were placed into the precooled FS device and after about 1 h the lids tightened and FS was performed for at least 8 h at -80 to -90°C; warming up to -55°C at a rate of 5-10°C per hour, subsequent post-fixation and staining at -55°C for 6 h, followed by warming up to -30°C at a rate of 5–10°C per hour where samples were left for an additional 3 h. Finally, samples were washed 3 times with acetone (10 min each), 16 h in 10% epoxy resin in acetone, 6 h in 30% epoxy resin in acetone, 16 h 70% epoxy resin in acetone, 6 h 100% epoxy resin in acetone, 16 h 100% epoxy resin in acetone. Then the samples were placed in fresh resin and placed in oven at 60° C overnight.

Sample serial thin (70nm) section of animals were cut with a diamond knife and mounted onto 150-200 mesh Hex grids. Ultrathin sections were examined with transmission EM Libra 120 EFTEM (Zeiss, Oberkochen, Germany) at 80 eV.

EV sizing and counting

Microfluidic Resistive Pulse Sensing (MRPS)[77]: measurements of isolated extracellular vesicle size and concentration were performed using the nCS1™ instrument (Spectradyne LLC, USA), which is based on the microfluidic resistive pulse sensing technology. EVs isolated from 250 polyps and resuspended in *Hydra* solution were diluted in equal volume with Tween/PBS buffer in order to meet the instrument requirements regarding medium conductivity. EV samples were analysed with TS-400 and TS-300 cartridges (measurement range 60 -400 nm and 50-300 nm, respectively).

Dynamic light scattering (DLS) was performed with a Malvern Zetasizer using EVs diluted in PBS at pH 7.4. Three runs were made at 25 °C and at 90°scattering angle.

Western blot analysis

Protein concentration was determined using a colorimetric assay based on the Bradford Assay (ThermoFisher) and samples were diluted with PBS to obtain equal protein concentration (EV and whole *Hydra* homogenates). Samples were mixed with 4x Laemmli Sample Buffer containing 2-mercaptoethanol (Biorad) and boiled for 5 min at 95°C. Proteins were resolved by SDS-PAGE (mini protean TGX precast any KDa gel (Biorad)), blotted onto PVDF membranes (Amersham) and blocked o/n at 4ºC in 5% non-fat dry milk in PBS-T (0.5% Tween-20). Membranes were then incubated with the primary antibody for 2 h at room temperature, washed with PBS-T 0.1%, and incubated with goat anti-rabbit IgG Antibody, (H+L) HRP-conjugated secondary antibody (1:4000, BioRad) for 1 h at room temperature. Finally, protein bands were detected using an enhanced chemiluminescence reagent (Clarity ECL Substrate (Biorad)) and imaged with ChemiDoc XRS *System* (BioRad,) using Image Lab software (BioRad). Antibodies: rabbit anti-CD63 (1:1000, System Biosciences), *Hydra* anti-Annexin B12 (kindly gifted by Dr. M. Isas, Keck School of Medicine of USC Los Angeles, CA), mouse anti-β-Actin–Peroxidase (1:40000, Sigma)

EV staining and uptake

EVs obtained as described before were labelled with PKH67 Green Fluorescent Cell Linker (Sigma Aldrich) following manufacturer's protocol, with minor modifications. Briefly, EVs obtained from 500 polyps in *Hydra* medium were added to 1

mL of diluent C. As a negative control, 1 mL of diluent C was mixed with the same volume of *Hydra* medium. Afterwards, 6 µL of PKH67 dye was added and mixed for 30 sec by gently pipetting. After 5 min incubation at room temperature, 2 mL of 10% BSA was added to quench the unbound dye. EVs were washed and isolated by ultracentrifugation as described before. *Hydra* were incubated with PKH67- labelled EVs and the negative control up to 5 h, washed with *Hydra* medium and imaged under a fluorescence microscope (Zeiss).

-

Regeneration Experiments

All the experiments were carried out using adult polyps starved for 24 h. For the head regeneration experiments, batches of 25 budless polyps were bisected at 80 % body length (sub-hypostomal cut) or 50 % body length (mid-gastric cut) and left regenerating for up to 72 h in presence of EVs isolated from 250 polyps and resuspended in 300 µL of *Hydra* solution. The regeneration process was monitored at different time points using an optical microscope and polyps were grouped into four stages according to their tentacle morphogenetic features.

For the foot regeneration experiments, groups of 15 animals were bisected at 20 % body length and transferred in 300 µL of *Hydra* solution containing EVs isolated from 250 polyps. After 24 h, polyps were relaxed in 2% urethane in *Hydra* medium (HM) for 2 min and pre-fixed by adding 4% PFA/HM for 15 min. After removing the pre-fixation medium, animals were fixed for 1-3 h in 4 % PFA/HM at 18°C and washed three times in PBS to remove any residual fixative. For the peroxidase assay, 2 mL of DAB solution was prepared according to the manufacturer's instructions (Sigma-Aldrich tablets) and used for 15 min on the fixed animals. In order to stop the colorimetric reaction, the polyps were washed five times with ddH_2O and then mounted with PBS/Glycerol 1:1 on microscope slides for imaging.

Stained animals were observed by an inverted microscope (Axiovert 100, Zeiss) and images of each foot were taken with a digital camera (Olympus, DP 70) under the same conditions of acquisition (light and exposure time). The colorimetric analysis was performed using the HSB format on the acquired images in the ImageJ software version 1.53e. Three staining categories were arbitrarily set according to DAB positive area extension as low (0-9000 mm^2), medium (9000-19000 mm^2) and high (19000-28000 mm^2).

EV pre-treatment with proteinase and RNAse

Prior to total RNA extraction, EVs isolated by ultracentrifugation were enzymatically treated to eliminate the free RNA derived from the ribonucleoprotein complexes that could be present in the conditioned medium. Isolated vesicles were treated with 1 mg/mL of proteinase K for 30 min at 37°C. Afterward, the samples were incubated 10 min at 65°C to inactivate the proteinase K and then treated with 10 µg/mL of RNAse A for 15 min at 37°C.

-

qRT-PCR Analysis

After treating polyps for 24 and 48 h with EVs isolated from 750 Hydra, total RNA was extracted from animals using Trizol or from EVs using Total RNA Extraction Kit (Norgen Biotek, Corp.) following manufacturer's instructions and its concentration was determined using a SmartSpec plus spectrophotometer (Biorad). The first-strand cDNA was synthesized by High Capacity cDNA Reverse Transcription Kit (Applied Biosystem). qRT-PCR was performed using a Fast SYBR™ Green Master Mix with premixed ROX (Applied Biosystems), in a StepOne Real-Time PCR System (Applied Biosystem) under the following fast cycling steps: initial denaturation for 20 s at 95°C, followed by 40 cycles at 95°C for 3 s, 60°C for 30 s. In addition, melting curves (20 min, from 59° to 90°C) were generated to check any undesired amplification products. EF1a was used as internal control.

In order to validate RNA-seq analysis, a presence/absence experiment of selected targets was performed using an EV sample isolated from 2000 polyps overall. Specific primers of *Hydra* genes *Wnt3a, b-catenin, actin and Hsp70* were designed using the Primer3 software (http://frodo.wi.mit.edu/primer3/) and are listed in Table S3, together with the corresponding GenBank accession numbers. Due to the qualitative nature of the presence/absence analysis, no internal control was used for the amplification reaction. The presence of such transcripts in the EV sample was confirmed by their cDNA amplification compared to negative controls, where no amplification occurred. Additional analysis by generation of melting curves (from 60 °C to 95 °C, 0.5 °C increment) confirmed sequence specific amplification in EVs and the absence of amplification in No Template Control (NTC). Mean C_t values for each gene and its NTC are shown in Table S2

RNA seq

EVs were collected at different times and stored at – 80 °C. Total RNA extraction was performed on EV samples collected from 10,000 polyps overall and in two replicates using “Total RNA Purification Kit” (Norgen Biotek Corp.) and following the manufacturer’s supplementary protocol for exosomal RNA purification, with one modification: the optional DNA removal step was carried out using RQ1 RNase-Free DNAse (Promega) at 0.1 U/mL. The two samples were sent to the Sequentia Biotech company for quality check, cDNA library preparation using “Ovation® SoLo RNA-Seq Systems” (NuGEN Technologies, Inc), and sequencing via a paired-end chemistry on an Illumina platform. After quality inspection of the produced reads with fastqc (https://www.bioinformatics.babraham.ac.uk/projects/trim_galore), reads were cleaned to remove the first 5 bases of read1, the Illumina adapter sequence 'AGATCGGAAGAGC' and the bases with quality below 20 from the 3’ end using the program TrimGalore! (https://www.bioinformatics.babraham.ac.uk/projects/trim_galore); the cleaned reads shorter than 35bp were removed from further analysis (9.3% of the produced read pairs). Trimmed reads were then aligned using the program STAR (version 2.7.1a) [78] against the NCBI *Hydra vulgaris* reference genome (assembly Hydra_RP_1.0), while for gene expression quantification, trimmed reads were also aligned on the corresponding transcript sequences GCF_000004095.1_Hydra_RP_1.0_rna.fna.gz using the program kallisto [78, 79]. Kallisto was also used to quantify genes using the reference transcriptome used in Siebert et al. [59] in order to directly map the genes with the cell types where they were identified.

Protein Identification by MALDI-TOF/TOF

To perform the MALDI-TOF EV samples were first run into a SDS-Page gel. EV total proteins were quantified using a Bradford assay, 4x Laemmli Sample Buffer with 2-mercaptoethanol (Biorad) was added, samples were heated to 95 °C for 5 min and they were run in a mini protean TGX precast 7.5% gel (Biorad). The gel was silver stained following standard procedures.

In-gel digestion- Protein bands were manually excised with a cutter, and in-gel digested with an automatic digestor (Intavis, Bioanalytical Instruments, Cologne, Germany). Briefly, spots were washed with water, ammonium bicarbonate (100 mM), and acetonitrile. Next, samples were reduced by incubation with DTT (10 mM) at 60 °C for 45 min and alkylated by incubation with iodoacetamide (50 mM) at room temperature for 30 min. Finally, proteins were digested with trypsin overnight at 37 °C (5 ng/µl, Trypsin Gold, Promega, WI, USA). Digestion was stopped by adding 0.5% TFA (trifluoroacetic acid), and tryptic peptides were extracted sequentially with increasing concentrations of acetonitrile in water. Peptides were concentrated and desalted by passing it through ZipTip C18 tips (Millipore) following the manufacturer’s instructions and eluted with 50%ACN 0.1%TFA.

Peptides were spotted into an Opti-Tof 384 well insert plate (Sciex) with a saturated solution of alpha-cyano-4-hydroxycinnamic acid (CHCA) prepared in 50% ACN/ 0.1% TFA. Proteins were identified using a 4800plus MALDI-TOFTOF (Sciex) in the reflector mode with accelerating voltage of 20 kV, mass range of 800–4000Da and 1000 shots/spectrum.

MS/MS spectra were acquired automatically on the 20 most intense precursors. Spectra were calibrated externally using a standard protein mixture (4700 Calmix, ABSciex).

Protein identification

Proteins were identified with the search engine Mascot (Matrix Science, London, UK) against the NCBIprot database of *Hydra* (29584 sequences). Search parameters used were: missed cleavage 1, fixed modifications carbamidomethyl (cysteines), variable modifications oxidation (methionine) and peptide and fragment mass tolerance 0.2 Da and 0.3 Da, respectively. Proteins with a score above 23 were considered a positive hit.

Protein Identification by LC-ESI-MS/MS

In solution digestion- Samples were evaporated and resuspended in 10 µl of denaturing buffer (6 M urea, 100 mM Tris buffer pH 7.8). Next, cysteins were reduced with 1.5 µl DTT (200 mM) for 30 min at 37 ºC and alkylated with 6 µl of iodoacetamide (200 mM) for 30 min in the dark. Unreacted iodoacetamide were consumed adding 6 µl of the reducing agent (200 mM DTT) for 30 min at room temperature. Samples were diluted with 50 mM ammonium bicarbonate to a final concentration less than 1M of urea. Digestion was carried out overnight with the enzyme trypsin (Gold Trypsin, Promega) at 37 °C and a 1:10 ratio (enzyme/protein). Reaction was stopped adding concentrated formic acid (Sigma). Samples were evaporated, resuspended in 2% acetonitrile, 0.1% formic acid and filtered through 0.45 µm filters. Protein identification was performed on a nano-LC system (Tempo MDLC, Eksigent, Dublin, CA, USA) coupled to a hybrid triple quadrupole/linear ion trap mass spectrometer (4000 QTRAP, Sciex). After precolumn desalting, tryptic digests (1 µg) were separated on a C18 column (Acclaim PepMap100, 75 µm id, 15 cm, 3 µm particle size, Thermo Scientific, USA) at a flow rate of 300 nL/min and a 120 min linear gradient from 5 to 35% ACN in 0.1% formic acid. The mass spectrometer was interfaced with a nanospray source equipped with uncoated fused silica emitter tip (20 µm inner diameter, 10 µm tip, NewObjective, Woburn, MA) and was operated in the positive ion mode. MS source parameters were as follows: capillary voltage 2800 V, source temperature 150 °C, declustering potential (DP) 85 V, curtain and ion source gas (nitrogen) 20 psi, and collision gas (nitrogen) high. Analyses were performed using an information dependent acquisition (IDA) method with the following steps: single enhanced mass spectra (EMS, 400–1400 m/z) from which the 8 most intense peaks were subjected to an enhanced product ion [EPI (MS/MS)] scan. Proteins were identified with the search engine Mascot (v2.3 MatrixScience, UK) using NCBIprot database of *Hydra* (29584 sequences). Search parameters used were: missed cleavages 1, fixed modifications carbamidomethyl (cysteines), variable modification oxidation (methionine) and peptide and fragment mass tolerance 0.5 and 0.3 Da, respectively. Only proteins with an overall Mascot score higher than 32 and at least 2 matching spectra were considered in the final list.

Declarations

Data availability

Proteomic data were submitted to PRoteomics IDEntifications (PRIDE) database. RNA-seq data were deposited in NCBI's Gene Expression Omnibus (GEO) and are accessible through GEO Series accession number GSE180886

Acknowledgments

Proteomic analyses were performed in the Proteomics Platform of Servicios Científico Técnicos del CIBA (IACS-Universidad de Zaragoza), ProteoRed ISCIII member. The authors acknowledge Prof. Mario Isas, Keck School of Medicine of USC Los Angeles, CA for the kind gift of *Hydra* anti-annexin B12 antibody. G.Tommasini thanks the MIUR project SHARID - ARS01-01270 for financial support. M.Moros acknowledges financial support from the European Research Council (ERC) under the European Union's Horizon 2020 research and innovation programme (grant agreement No 853468), from the European

Union's Horizon 2020 research and innovation programme under the Marie Skłodowska-Curie grant agreement No. 660228 and from the Spanish Ministry of Science and Innovation through the Ramón y Cajal grant RyC2019- 026860-I.

Author contribution

C.T. conceived the project, designed, and supervised research. M.M[*], E.F., G.T., G.P. and A.A. performed EV isolation and Hydra experiments. V.M. performed TEM characterization. B.M. performed qRT-PCR. E.F performed functional analyses. M.M.[#] performed bioinformatic analyses. A.T. and M.M[*]analysed data and supervised research. C.T. wrote the manuscript with contributes from all authors.

[*] Maria Moros, [#] Margherita Mutarelli

References

1. Misu A*, et al.* Two Different Functions of Connexin43 Confer Two Different Bone Phenotypes in Zebrafish. *The Journal of biological chemistry* **291**, 12601-12611 (2016).

2. Takaku Y*, et al.* Innexin gap junctions in nerve cells coordinate spontaneous contractile behavior in Hydra polyps. *Scientific reports* **4**, 3573 (2014).

3. Zong L, Zhu Y, Liang R, Zhao HB. Gap junction mediated miRNA intercellular transfer and gene regulation: A novel mechanism for intercellular genetic communication. *Scientific reports* **6**, 19884 (2016).

4. Thery C, Witwer KW, Aikawa E, Alcaraz MJ, Anderson JD. Minimal information for studies of extracellular vesicles 2018 (MISEV2018): a position statement of the International Society for Extracellular Vesicles and update of the MISEV2014 guidelines. *Journal of extracellular vesicles* **7**, 1535750 (2018).

5. Veziroglu EM, Mias, G. Characterizing Extracellular Vesicles and Their Diverse RNA Contents *Frontiers genetics* **11**, 700 (2020).

6. Kalra H SR, Ji H, Aikawa E, Altevogt P, Askenase P, et al. Vesiclepedia: A Compendium for Extracellular Vesicles with Continuous Community Annotation. *Plos biology* **10**, e1001450 (2012).

7. Pan BTJ, R.M. . Fate of the transferrin receptor during maturation of sheep reticulocytes in vitro: Selective externalization of the receptor. . *Cell* **33**, 967-978 (1983).

8. Harding C HJ, Stahl P. . Endocytosis and intracellular processing of transferrin and colloidal gold-transferrin in rat reticulocytes: demonstration of a pathway for receptor shedding. *Eur J Cell Biol* **35**, 256-263 (1984).

9. Johnstone RM, M. A, R. HJ, L. O, C. T. Vesicle Formation during Reticulocyte Maturation - Association of Plasma-Membrane Activities with Released Vesicles (Exosomes). *The Journal of biological chemistry* **262**, 9412-9420 (1987).

10. Skryabin GO, Komelkov AV, Savelyeva EE, Tchevkina EM. Lipid Rafts in Exosome Biogenesis. *Biochemistry Biokhimiia* **85**, 177-191 (2020).

11. Colombo M, Raposo G, Thery C. Biogenesis, secretion, and intercellular interactions of exosomes and other extracellular vesicles. *Annual review of cell and developmental biology* **30**, 255-289 (2014).

12. Kalluri R, LeBleu VS. The biology, function and biomedical applications of exosomes. *Science* **367**, eaau6977 (2020).

13. Anand S, Samuel M, Kumar S, Mathivanan S. Ticket to a bubble ride: Cargo sorting into exosomes and extracellular vesicles. *Biochimica et biophysica acta Proteins and proteomics* **1867**, 140203 (2019).

14. Kowal J*, et al.* Proteomic comparison defines novel markers to characterize heterogeneous populations of extracellular vesicle subtypes. *Proceedings of the National Academy of Sciences of the United States of America* **113**, E968-977 (2016).

15. Juan T, Furthauer M. Biogenesis and function of ESCRT-dependent extracellular vesicles. *Seminars in cell & developmental biology* **74**, 66-77 (2018).

16. Ludwig N, Whiteside TL, Reichert TE. Challenges in Exosome Isolation and Analysis in Health and Disease. *International journal of molecular sciences* **20**, (2019).

17. Coakley G, Maizels RM, Buck AH. Exosomes and Other Extracellular Vesicles: The New Communicators in Parasite Infections. *Trends Parasitol* **31**, 477-489 (2015).

18. Peinado H*, et al.* Melanoma exosomes educate bone marrow progenitor cells toward a pro-metastatic phenotype through MET. *Nature Medicine* **18**, 883-891 (2012).

19. Ghajar CM*, et al.* The perivascular niche regulates breast tumour dormancy. *Nature Cell Biology* **15**, 807-817 (2013).

20. Peinado H*, et al.* Pre-metastatic niches: organ-specific homes for metastases. *Nature Reviews Cancer* **17**, 302-317 (2017).

21. Lu M, Huang Y. Bioinspired exosome-like therapeutics and delivery nanoplatforms. *Biomaterials* **242**, 119925 (2020).

22. Gradilla AC*, et al.* Exosomes as Hedgehog carriers in cytoneme-mediated transport and secretion. *Nature communications* **5**, 5649 (2014).

23. Gross JC, Chaudhary V, Bartscherer K, Boutros M. Active Wnt proteins are secreted on exosomes. *Nature cell biology* **14**, 1036-1045 (2012).

24. Liegeois S, Benedetto A, Garnier JM, Schwab Y, Labouesse M. The V0-ATPase mediates apical secretion of exosomes containing Hedgehog-related proteins in Caenorhabditis elegans. *The Journal of cell biology* **173**, 949-961 (2006).

25. Wehman AM, Poggioli, C., Schweinsberg, P., Grant, B. D., Nance, J. The P4-ATPase TAT-5 inhibits the budding of extracellular vesicles in C. elegans embryos. *Curr Biol* **21**, 1951-1959 (2011).

26. Schatz D, Vardi A. Extracellular vesicles — new players in cell–cell communication in aquatic environments. *Current Opinion in Microbiology* **43**, 148-154 (2018).

27. Allocca M*, et al.* An Integrated Multilevel Analysis Profiling Biosafety and Toxicity Induced by Indium- and Cadmium-Based Quantum Dots in Vivo. *Environmental science & technology* **53**, 3938-3947 (2019).

28. Ambrosone A*, et al.* Dissecting common and divergent molecular pathways elicited by CdSe/ZnS quantum dots in freshwater and marine sentinel invertebrates. *Nanotoxicology* **11**, 289-303 (2017).

29. Quinn B, Gagnè F, Blaise C. Hydra, a model system for environmental studies. *The International journal of developmental biology* **56**, 613-625 (2012).

30. Tortiglione C*, et al.* Semiconducting polymers are light nanotransducers in eyeless animals. *Sci Adv* **3**, e1601699 (2017).

31. Veronesi G*, et al.* In Vivo Biotransformations of Indium Phosphide Quantum Dots Revealed by X-Ray Microspectroscopy. *ACS applied materials & interfaces* **11**, 35630-35640 (2019).

32. Moros M*, et al.* In Vivo Bioengineering of Fluorescent Conductive Protein-Dye Microfibers. *iScience* **23**, 101022 (2020).

33. Moros M*, et al.* Gold Nanorods and Nanoprisms Mediate Different Photothermal Cell Death Mechanisms In Vitro and In Vivo. *ACS Appl Mater Interfaces* **12**, 13718-13730 (2020).

34. Bosch TC. Hydra and the evolution of stem cells. *BioEssays : news and reviews in molecular, cellular and developmental biology* **31**, 478-486 (2009).

35. Hobmayer B*, et al.* Stemness in Hydra - a current perspective. *The International journal of developmental biology* **56**, 509-517 (2012).

36. Steele RE. Developmental signaling in Hydra: what does it take to build a "simple" animal? *Developmental biology* **248**, 199-219 (2002).

37. Vogg MC, Galliot B, Tsiairis CD. Model systems for regeneration: Hydra. *Development* **146**, (2019).

38. Bode HR. Head regeneration in Hydra. *Dev Dyn* **226**, 225-236 (2003).

39. Li Q, Yang H, Zhong TP. Regeneration across metazoan phylogeny: lessons from model organisms. *J Genet Genomics* **42**, 57-70 (2015).

40. Hobmayer B*, et al.* WNT signalling molecules act in axis formation in the diploblastic metazoan Hydra. *Nature* **407**, 186-189 (2000).

41. Chera S*, et al.* Apoptotic cells provide an unexpected source of Wnt3 signaling to drive hydra head regeneration. *Developmental cell* **17**, 279-289 (2009).

42. Lengfeld T*, et al.* Multiple Wnts are involved in Hydra organizer formation and regeneration. *Developmental biology* **330**, 186-199 (2009).

43. Münder S*, et al.* Notch-signalling is required for head regeneration and tentacle patterning in Hydra. *Developmental biology* **383**, 146-157 (2013).

44. Cazet JF, Cho A, Juliano CE. Generic injuries are sufficient to induce ectopic Wnt organizers in Hydra. *Elife* **10**, (2021).

45. Petersen HO*, et al.* A Comprehensive Transcriptomic and Proteomic Analysis of Hydra Head Regeneration. *Molecular biology and evolution* **32**, 1928-1947 (2015).

46. Bode HR. Axial patterning in hydra. *Cold Spring Harbor perspectives in biology* **1**, a000463 (2009).

47. Gufler S*, et al.* beta-Catenin acts in a position-independent regeneration response in the simple eumetazoan Hydra. *Developmental biology* **433**, 310-323 (2018).

48. Wenger Y, Buzgariu W, Perruchoud C, Loichot G, Galliot B. Generic and context-dependent gene modulations during Hydra whole body regeneration. *bioRxiv*, 587147 (2019).

49. Macwilliams HK. Hydra Transplantation Phenomena and the Mechanism of Hydra Head Regeneration .1. Properties of the Head Inhibition. *Developmental biology* **96**, 217-238 (1983).

50. Macwilliams HK. Hydra Transplantation Phenomena and the Mechanism of Hydra Head Regeneration .2. Properties of the Head Activation. *Developmental biology* **96**, 239-257 (1983).

51. McGough IJ, Vincent J-P. Exosomes in developmental signalling. *Development* **143**, 2482 (2016).

52. Zhang L, Wrana JL. The emerging role of exosomes in Wnt secretion and transport. *Current Opinion in Genetics & Development* **27**, 14-19 (2014).

53. C Thery AC, S Amigorena, G Raposo. *Isolation and Characterization of Exosomes from Cell Culture Supernatants and Biological Fluids*. John Wiley & Sons, Inc. (2006).

54. Rutter BD, Innes RW. Growing pains: addressing the pitfalls of plant extracellular vesicle research. *New Phytol* **228**, 1505-1510 (2020).

55. Marchesano V*, et al.* Imaging inward and outward trafficking of gold nanoparticles in whole animals. *ACS nano* **7**, 2431-2442 (2013).

56. Lommel M*, et al.* Hydra Mesoglea Proteome Identifies Thrombospondin as a Conserved Component Active in Head Organizer Restriction. *Scientific Reports* **8**, (2018).

57. Kriventseva EV*, et al.* OrthoDB v10: sampling the diversity of animal, plant, fungal, protist, bacterial and viral genomes for evolutionary and functional annotations of orthologs. *Nucleic Acids Res* **47**, D807-D811 (2019).

58. Huang XY*, et al.* Characterization of human plasma-derived exosomal RNAs by deep sequencing. *Bmc Genomics* **14**, (2013).

59. Siebert S*, et al.* Stem cell differentiation trajectories in Hydra resolved at single-cell resolution. *Science* **365**, 341-+ (2019).

60. Guder C*, et al.* An ancient Wnt-dickkopf antagonism in Hydra. *Development* **133**, 901-911 (2006).

61. Augustin R*, et al.* Dickkopf related genes are components of the positional value gradient in hydra. *Developmental Biology* **296**, 62-70 (2006).

62. Ziegler B*, et al.* The Wnt-specific astacin proteinase HAS-7 restricts head organizer formation in Hydra. *Bmc Biol* **19**, (2021).

63. Vogg MC*, et al.* An evolutionarily-conserved Wnt3/beta-catenin/Sp5 feedback loop restricts head organizer activity in Hydra. *Nature Communications* **10**, (2019).

64. Hoffmeister S, Schaller HC. A New Biochemical Marker for Foot-Specific Cell-Differentiation in Hydra. *Roux Arch Dev Biol* **194**, 453-461 (1985).

65. Cruz L, Romero JAA, Iglesia RP, Lopes MH. Extracellular Vesicles: Decoding a New Language for Cellular Communication in Early Embryonic Development. *Frontiers in cell and developmental biology* **6**, 94 (2018).

66. Buck AH*, et al.* Exosomes secreted by nematode parasites transfer small RNAs to mammalian cells and modulate innate immunity. *Nature communications* **5**, 5488 (2014).

67. Cai Q, He B, Weiberg A, Buck AH, Jin H. Small RNAs and extracellular vesicles: New mechanisms of cross-species communication and innovative tools for disease control. *PLoS pathogens* **15**, e1008090 (2019).

68. Woith E, Fuhrmann G, Melzig MF. Extracellular Vesicles-Connecting Kingdoms. *International journal of molecular sciences* **20**, (2019).

69. Gill S, Catchpole R, Forterre P. Extracellular membrane vesicles in the three domains of life and beyond. *FEMS microbiology reviews* **43**, 273-303 (2019).

70. Broun M, Gee L, Reinhardt B, Bode HR. Formation of the head organizer in hydra involves the canonical Wnt pathway. *Development* **132**, 2907-2916 (2005).

71. Gee L*, et al.* beta-catenin plays a central role in setting up the head organizer in hydra. *Dev Biol* **340**, 116-124 (2010).

72. Munder S*, et al.* Notch-signalling is required for head regeneration and tentacle patterning in Hydra. *Dev Biol* **383**, 146-157 (2013).

73. Doyle LM, Wang MZ. Overview of Extracellular Vesicles, Their Origin, Composition, Purpose, and Methods for Exosome Isolation and Analysis. *Cells* **8**, (2019).

74. Jeppesen DK*, et al.* Reassessment of Exosome Composition. *Cell* **177**, 428-445 e418 (2019).

75. Dupre C, Yuste R. Non-overlapping Neural Networks in Hydra vulgaris. *Curr Biol* **27**, 1085-1097 (2017).

76. Théry C AS, Raposo G, Clayton A. . Isolation and Characterization of Exosomes from Cell Culture Supernatants and Biological Fluids In: *Curr Protoc Cell Biol.*) (2006).

77. Cleland AN, Fraikin, J.-L., Meinhold, P., and Monzon, F. 6:20. Nanoparticle characterization—one size does not fit all: nanoparticle size analysis for nanomedicine applications. . *Drug Dev Deliv*, 20 (2016).

78. Dobin A*, et al.* STAR: ultrafast universal RNA-seq aligner. *Bioinformatics* **29**, 15-21 (2013).

79. Bray NL, Pimentel H, Melsted P, Pachter L. Near-optimal probabilistic RNA-seq quantification (vol 34, pg 525, 2016). *Nat Biotechnol* **34**, 888-888 (2016).

Figures

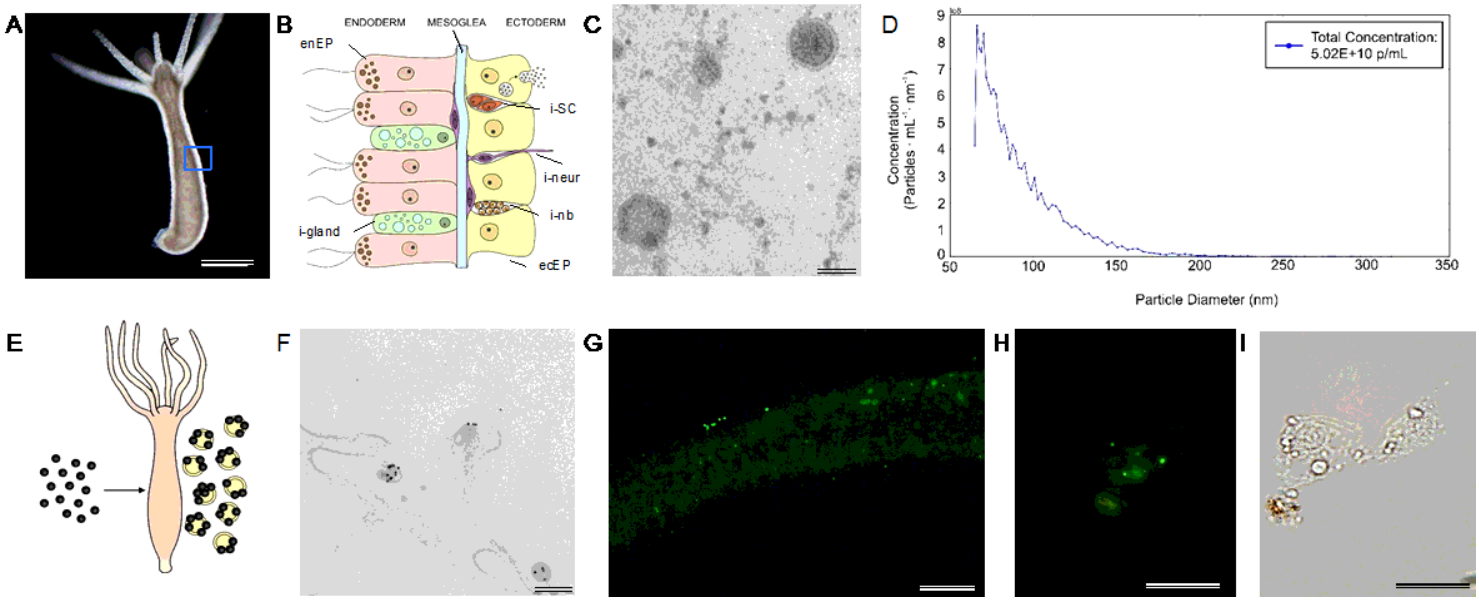

Figure 1

Morphological characterization of Hydra EV. A) Bright field image of a living Hydra vulgaris showing the simple body plan and B) a schematic representation of the diploblastic tissue organization in a cross-section view. Epitheliomuscular cells (ecEp, yellow) face the outer medium and the inner cavity (enEp, pink). Interstitial stem cells (iSC, orange) lay interspersed into the ectoderm giving rise to a few differentiated cell types such as nematoblasts (i-nb), neurons (i-neur) and gland cells (i-gland). EV release into the medium is shown for a single ectodermal cell. C) TEM image of isolated vesicles exhibiting round morphology and a bilayered membrane. Scale bar, 50 nm. D) MRPS measurements show the distribution of the EV size, presenting two major peaks at 66 and 70,5 nm (using a TS-400 cartridge). E) Schematic illustration of in vivo assembling of AuNP decorated EV, by treatment of Hydra with AuNPs. F) TEM analysis 48 h post treatment shows AuNPs on the surface of EVs. Scale bar 200 nm. G) PKH67 labelled-EVs were incubated 2 h with living Hydra. The picture shows the body column with green fluorescent granular signals, clearly detectable also on fixed single cells H) obtained by maceration of treated polyps. I) Bright field image of the same cell. Scale bar 200 µm in G, 20 µm in H, I.

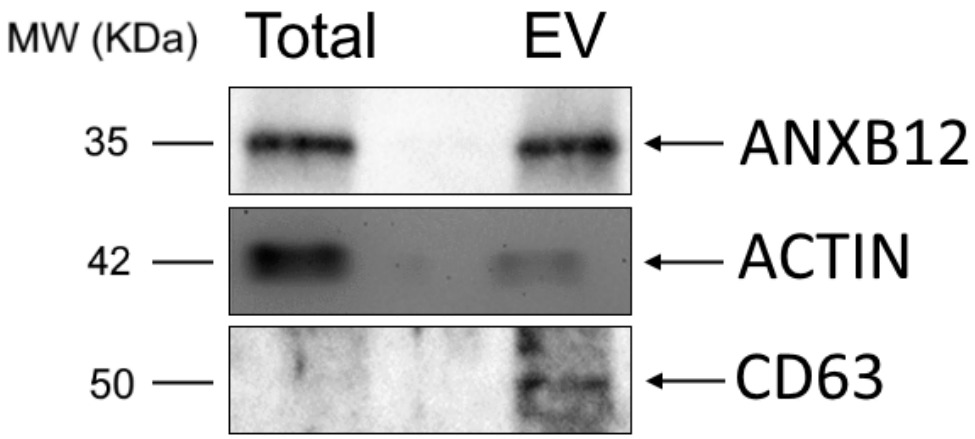

Figure 2

Protein identification in Hydra EV Western blot analysis of typical exosome biomarkers in whole-body protein extracts (Total) and EV fractions (EV) shows specific cross reactions to Hydra anti Annexin B12, mouse anti actin and rabbit anti CD63 antibodies. An enrichment in the exosome specific marker CD63 was observed in EV protein extracts, compared to whole body lysates.

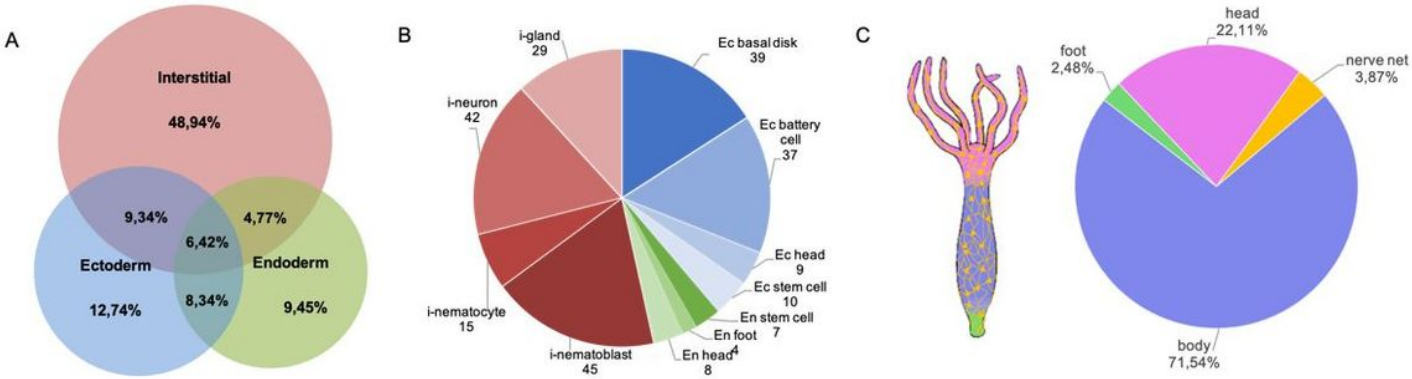

Figure 3

Molecular contribution of cell lineages to EV transcriptome A) Venn Diagram showing cell lineage contribution to EV transcriptome. The clusters of cells included into each cell lineage were identified by scRNA-seq analysis recently reported 59 and are listed in Supplementary Fig S5. B) Distribution EV transcripts matching the scRNA-seq atlas, subclustered according to their unique presence in a specific cell type of ectoderm (blue tones), interstitial (red tones) and endodermal (green tone) cell lineage. Transcripts common to multiple cell lineages are not included. C) Anatomical source of EV transcripts. The distribution shows EV transcripts derived from all body regions, including neurons.

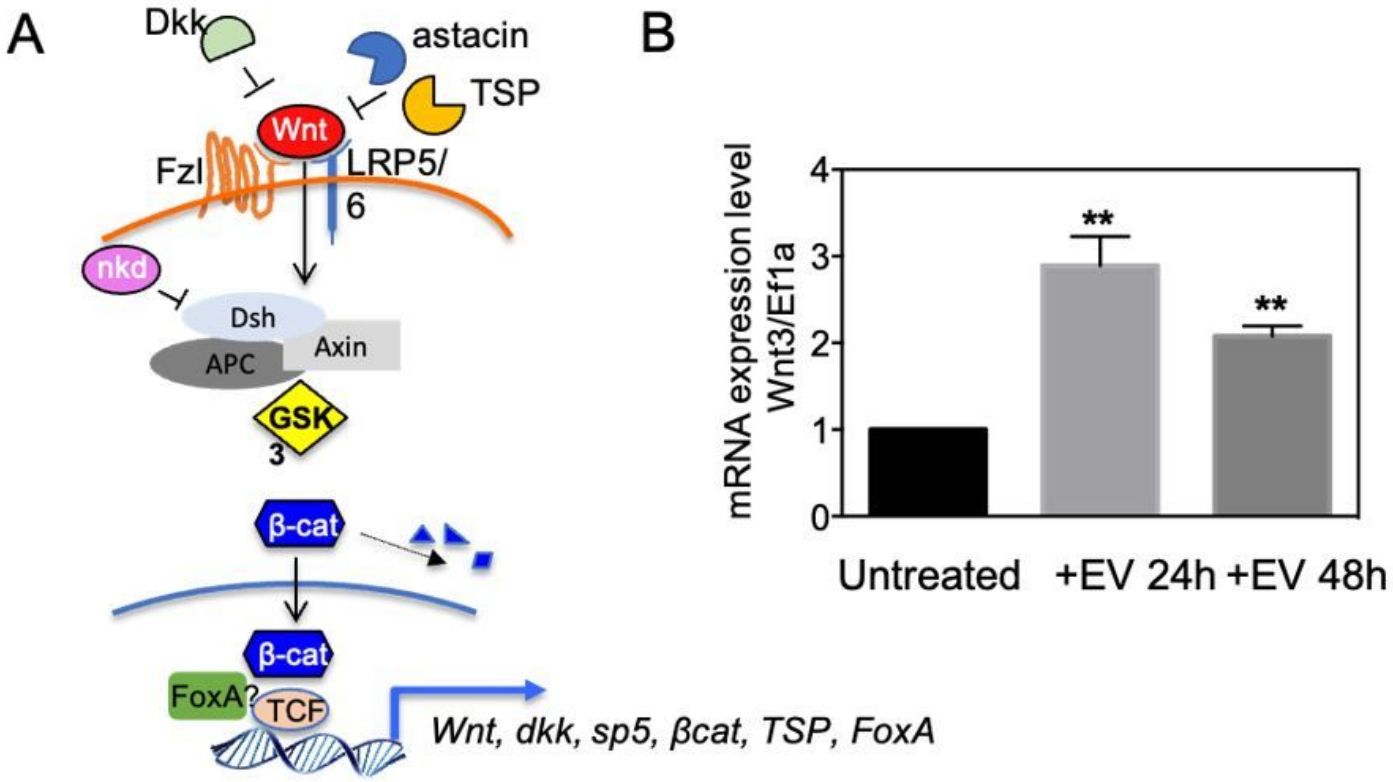

Figure 4

Wnt signaling activation via Hydra EV A) Schematic view of the canonical Wnt/β-catenin pathway at cellular level, in the activated state, showing extracellular and intracellular regulators identified in the Hydra EV transcriptome. B) Relative mRNA expression levels of Wnt3/Ef1α. Whole polyps were treated for the indicated period with EVs freshly isolated from Hydra medium, then processed for RNA extraction and qRT-PCR. Data represent the average of three biological replicates, each performed in triplicate. Statistical evaluation was performed using the One sample t test, **P<0.005

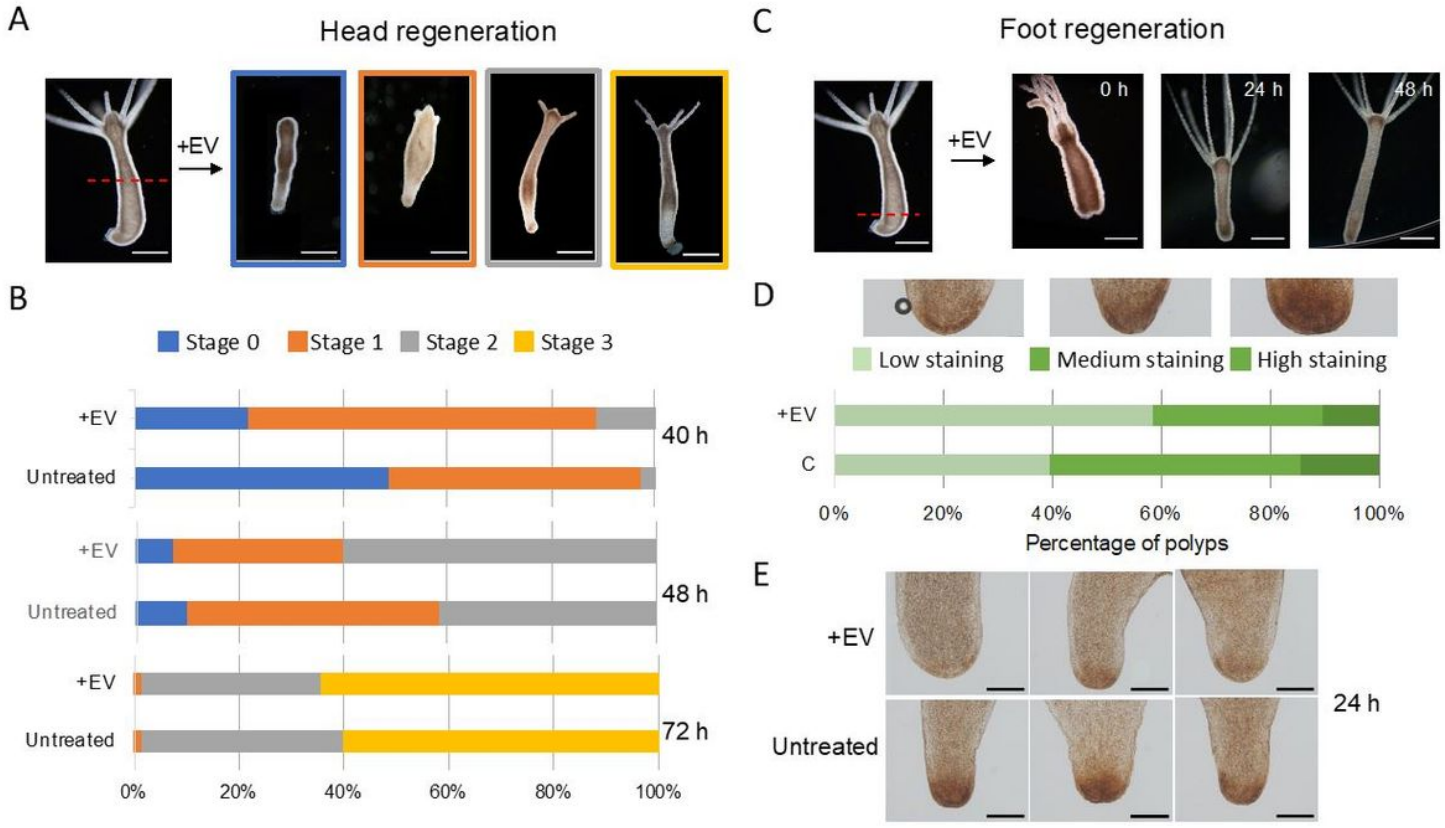

Figure 5

Hydra head and foot regeneration are modulated by EV A) Light microscopy images of regenerating polyps, grouped in four categories according to progressive developmental stage. B) Histograms report the distribution of developmental stages at 40 h, 48 h and 72 h post midgastric amputation (shown by the red dotted line). The bar color corresponds to the regenerative stages shown in A. Data represent the average of three independent experiments (n= 70). Differences in the distributions of untreated and treated polyps were statistically evaluated using Chi squared test. At 40 h $\chi 2 = 39.353$ with 2 degrees of freedom. Two-tailed ***P value < 0.0001; at 48 h $\chi 2 = 9.958$ with 2 degrees of freedom. Two-tailed *P value = 0.0069; not significant differences resulted at 72 h $\chi 2$ 0.548 with 2 degrees of freedom. The two-tailed P value equals 0.7605 C) Light microscopy images of foot regenerates at different time post amputation (red dotted line). D) Distribution of foot regenerating polyps grouped in three categories: light, medium and dark green, corresponding to low, medium and high peroxidase staining, determined as DAB positive area by using Image J. Experiments were performed in triplicate (n=45). $\chi 2 = 7.062$ with 2 degrees of freedom. two-tailed *P < 0.05. E) Representative images of foot regenerating polyps (untreated and treated with EVs) 24 h p.a.

Supplementary Files

This is a list of supplementary files associated with this preprint. Click to download.

- supplementaryfile1GCF000004095.1HydraRP1.0.xlsx
- SupplementaryMaterialsComBiol.docx
- supplementaryfile2GHHG01scRNAseq.xlsx